Sustainable Marine Structures
https://journals.nasspublishing.com/sms

ARTICLE

Strain Hardening Monotonic and Cyclic Response of Cohesive Seabed through Bounding Surface Theory

Mehmet Barış Can Ülker

Institute of Disaster Management, Istanbul Technical University, Istanbul 34469, Turkey

ABSTRACT

Seabed soils' stress-strain relationships are nonlinear, and the complexity associated with soil constitutive behavior increases substantially as the loading becomes reversed. This study focuses on the constitutive behavior of cohesive seabed soils under monotonic and cyclic wave loadings. The theoretical framework developed is based on Bounding Surface Plasticity, where soil strain-hardening is addressed through a proposed hardening law to calculate plastic strains and their evolution during the loading history. Considering clays and clay-like cohesive soils located mainly on the surface of the seabed, the plastic hardening modulus is updated using deviatoric plastic strains, and a new degradation function, which is a novel contribution in the study, is developed and incorporated into the theoretical framework. The proposed model, whose mathematical formulation is more practical and simpler compared to other similar models for cohesive seabed soils, is integrated into a computer program using an explicit numerical scheme. Then, several drained and undrained monotonic and cyclic triaxial tests for normally and over-consolidated clays are simulated to verify the proposed constitutive formulation. Results indicate that simulations of cyclic triaxial tests using the proposed model successfully capture the essential static and dynamic behavior of cohesive seabed soils, including large number of load cycles. The proposed model stands out with its predictive power and the simplification advantage it brings to the theory through the hardening law compared to previous models, as successfully demonstrated in this study. The proposed model can be used in solving coastal and offshore geotechnical engineering problems with high accuracy.

*CORRESPONDING AUTHOR:
Mehmet Barış Can Ülker, Institute of Disaster Management, Istanbul Technical University, Istanbul 34469, Turkey;
Email: mbulker@itu.edu.tr

ARTICLE INFO
Received: 15 August 2025 | Revised: 29 October 2025 | Accepted: 3 November 2025 | Published Online: 29 December 2025
DOI: https://doi.org/10.36956/sms.v7i4.2640

CITATION
Ülker, M.B.C., 2025. Strain Hardening Monotonic and Cyclic Response of Cohesive Seabed through Bounding Surface Theory. Sustainable Marine Structures. 7(4): 276–294. DOI: https://doi.org/10.36956/sms.v7i4.2640

Keywords: Bounding Surface; Clays; Cyclic Shearing; Degradation; Hardening Law; Monotonic Response; Seabed

1. Introduction

Soils are inherently heterogeneous and complex multi-phase materials with a particulate structure. Understanding and predicting the nonlinear cyclic and monotonic behavior of soils under complex loading has been a major focus of geomechanical research for several decades. The constitutive behavior of cohesive soils has long been a subject of interest to researchers seeking to understand the fundamental characteristics of their response to various time-dependent loadings, such as earthquakes and waves. The nature of such research provides invaluable information for designing soil-structure systems against external effects. Early studies provided the foundation for constitutive models that could capture soil behavior beyond the assumptions of classical plasticity. In the laboratory, experiments are performed to measure soil properties irrespective of the soil type. While such an effort is often preferable, resulting in the most accurate values, it is not feasible to experiment each time there is a need for such soil data. Therefore, it is of utmost necessity to develop accurate constitutive theories to predict the actual soil static or dynamic response in a broad spectrum. Particularly, the stress-strain relationship and shear-strength characteristics of cohesive seabed soils need to be modeled using mathematical theories to solve related geotechnical engineering problems through numerical methods.

Among these theories, the multi-surface kinematic-hardening theory by Mroz[1] is one of the first successful ones, which was later improved[2–5]. These early models introduced the ability to represent cyclic hysteresis and strain accumulation under repeated loading, which are critical phenomena for offshore and earthquake engineering applications. By adopting two surfaces, such a model was independently proposed by Krieg[6] and Dafalias and Popov[7]. This theory later evolved into the "Bounding Surface Theory"[8–11]. Subsequent developments produced a range of elastoplastic, kinematic, and anisotropic hardening models, capable of describing liquefaction and other cyclic loading effects. Around that time, a bounding surface model was developed, introducing several deformation modes and the progressive generation of pore pressure in granular seabed soils by Pietruszczak and Poorooshasb[12] and Poorooshasb and Pietruszczak[13]. The study by Poorooshasb and Pietruszczak[14] simplified the model regarding its kinematic hardening rule. These works capture the overall cyclic behavior, including the pore pressure buildup, showing the robustness of the bounding surface theory. However, they were too complex with their hardening laws and inefficient in their numerical implementation. Despite their advances, Bounding Surface Models were limited in reproducing plastic deformation during unloading and stress reversal, restricting their applicability to strongly cyclic environments. To overcome these shortcomings, as an alternative to bounding surface models, Zienkiewicz and Mroz[15] developed the framework of generalized plasticity. A Bounding Surface Model was used for nonlinear analysis of seabed by Poorooshasb et al.[16] and then a comprehensive model was developed by Zienkiewicz et al.[17], and subsequently extended by Pastor et al.[18]. However, bounding surface plasticity allows plastic strains to be developed during loading-unloading cycles through plastic potential functions. Putting a bulk of earlier studies aside, Yao et al.[19] developed a model for over-consolidated reconstituted clays, considering the variation in the yield surface of structured clays. Later, Chen et al.[20] developed an elastoplastic model for structured clays accounting for the change in fabric post-yield deformation. These models exhibit rather more complex implementation procedures and do not model the entirety of cohesive soil behavior with high success. Cheng and Wang[21] proposed a total stress-based bounding surface model to predict the undrained behavior of saturated soft clays under cyclic loadings based on the anisotropic hardening modulus. Their model is not an effective stress-based model with a new hardening rule and a complex interpolation function. Park[22] examined the strength loss and the softening rate for weakly cemented clays for both artificially cemented high-plasticity clay and low-plasticity

soils. Their highly specialized study also characterizes the softening behavior of weakly cemented sensitive clay. Elia and Rouainia [23] studied the cyclic behavior of clays through a kinematic hardening model. Carlton and Pestana [24] developed a model for estimating various soils' in-situ small-strain shear modulus. Buchely et al. [25] proposed a model to investigate the high-strain behavior of clays, and Cuvilliez et al. [26] proposed an elastic-viscoplastic model for claystone response. Deng and Ren [27] studied energy methods for capturing the deformation behavior of soft clays. Although these models are effective for specific soils, they are highly specialized and do not accurately capture the monotonic and cyclic behavior of cohesive soils.

For clay-like seabed soils to be represented in numerical analyses, one needs to consider their nonlinear dynamic properties [28–30] under wave loading, even if it means using relatively simple elastic-plastic constitutive models [31]. Shi et al. [32] developed a hybrid flow rule for understanding cyclic clay response. More recently, Yao et al. [33] proposed a unified constitutive model for soils. Other most recent models attempt to capture the dynamic response of soils relying on many well-known theories, including multi-surface plasticity and bounding surface plasticity [34–40]. More recently, Liu and Xue [41] performed a series of undrained cyclic triaxial tests on kaolin clay to investigate strain accumulation under consecutive and intermittent loading patterns.

While these classical and advanced plasticity models have significantly improved the understanding of soil behavior under cyclic and monotonic loads, their integration into reliability frameworks and numerical codes for offshore structures remains limited. In particular, soil-structure interactions in offshore systems introduce coupled hydro-mechanical complexities such as evolving pore pressure, strain softening, and load redistribution—that are not fully captured by existing models. The problem is that these models cannot adequately simulate the cyclic softening and degradation behavior of soft clays. More advanced constitutive models for simulating the cyclic behavior of cohesive soils with varying levels of plasticity have been developed [42–50]. However, a need still remains to verify and validate these models, which are implemented in various software programs commonly used in our engineering practice. The problem with the current state of practice involving the development and use of constitutive theories associated with soils is that many advanced models for representing the stress-strain relationships of granular soils are available in finite element codes, whereas the models for cohesive soils achieving a successful predictive capability spanning various over-consolidation ratios in these codes are not that widespread. That is, engineers who urgently need accurate solutions to the problems in engineering practice face limited options. The same is the case for 'intermediate soils' such as low-plasticity silts, sandy silts, or sandy clays, whose cyclic responses are not well-understood compared to those that are reasonably captured by available constitutive models for sand-like or clay-like behaviors [35,51]. Thus, there is a constant need to seek the most efficient and accurate solution for the constitutive behavior of cohesive soils under both static and cyclic loadings. Also, among such existing models, simpler and more practical constitutive relations, in particular, hardening laws, are still necessary to capture the response of clays.

In this study, the monotonic and cyclic behavior of cohesive seabed soils are revisited through a simple yet robust constitutive model developed using the bounding surface plasticity framework. The hardening law addresses the soil's strain-hardening response, including a new interpolation function for evaluating the plastic hardening modulus based on plastic deviatoric strains. The developed hardening law is simpler compared to several others used to model similar seabed soils within the bounding surface or generalized plasticity models. This novel hardening law is then incorporated into the model, considering the essentials of the critical state soil mechanics, allowing the capture of the cyclic mobility of both normally and over-consolidated clays. While the presented model is more straightforward in its formulation with the proposed hardening law than the conventional Bounding Plasticity Theory, it is still sophisticated enough to capture the main features of clay soil response. In that sense, the proposed model has several advantages based on its theoretical foundations compared to earlier models with similar backgrounds, such as generalized plasticity. Also, the proposed hardening law re-

quires two parameters to be determined to capture the response of cohesive seabed soils. It should be mentioned that stress anisotropy and loading rate effects are not considered in the study.

2. Modeling Constitutive Behavior of Cohesive Soils

Modeling the constitutive behavior of cohesive soils differs from that of cohesionless soil behavior in that pore pressure generation stays limited, allowing plastic deformations to develop more rapidly in the soil. Similar to loose sands, clay-like soil undergoes elasto-plastic deformation when it is unloaded for the first time. Upon continued reloading-unloading cycles, the soil exhibits plastic strains until failure. Therefore, there is a significant need for a mechanism that distinguishes virgin loading behavior from that of stress reversals, also called non-virgin loading. In this section, the static and dynamic response of cohesive soils is modeled using a mathematical framework based on bounding surface plasticity, implemented explicitly within a computational domain.

2.1. Bounding Surface Formulation

2.1.1. Bounding Surface

In bounding surface plasticity, the variation of stress vector located on a 'loading or yield surface' is determined based on a stress counterpart located on the bounding surface, often called 'image stress,' which distinguishes between admissible and inadmissible stress states. Satisfying such a condition through the function taken in this study is:

$$F = (\sigma_m + \beta)^2 + 3\left(\frac{\bar{\sigma}}{m}\right)^2 - \bar{p}^2 = 0 \tag{1}$$

where the mean stress, deviatoric stress invariant, and the deviatoric component of the stress vector are defined respectively as:

$$\sigma_m = I_1 = \frac{\sigma_{ii}}{3},\ \bar{\sigma} = \sqrt{1/2 S_{ij} S_{ij}}\,,\ S_{ij} = \sigma_{ij} - \delta_{ij}\sigma_m \tag{2}$$

The other parameters are defined as,

$$m = M_c \frac{\beta}{\bar{p}}, \beta = \frac{p_c}{r}, \bar{p} = p_c - \beta \tag{3}$$

with M_c being the slope of the critical state line (CSL) on the compression side as in **Figure 1**; p_c, the pre-consolidation pressure, which acts as a hardening parameter, and is the ratio of the diameter of the ellipse to the distance of the center measured from the origin for the *F* function. In the case of triaxial stress state, which is utilized to simulate laboratory triaxial tests, we write $p = -\sigma_m$ and $q = -\sqrt{3}\sigma$. To be consistent with a potential Mohr-Coulomb type rule, M_c slope becomes,

$$M_c = 6t \sin\phi / (3t - \sin\phi) \tag{4}$$

where t takes + 1 for the compression test, and –1 for the extension test. The 'loading or yield surface', $f = 0$, having a similar form to (1), is,

$$f = \left(\widehat{\sigma}_m + \widehat{\beta}\right)^2 + 3\left(\frac{\widehat{\bar{\sigma}}}{\widehat{m}}\right)^2 - \widehat{p}^2 = 0 \tag{5}$$

where '$\bar{\sigma}$' indicates the stress on the loading surface; the same is true for other parameters also defined on the loading surface, *f*. The following are now redefined:

$$\widehat{m} = M_c \frac{\widehat{\beta}}{\widehat{p}}, \widehat{\beta} = \frac{\widehat{p}_c}{\widehat{r}}, \widehat{p} = \widehat{p}_c - \widehat{\beta} \tag{6}$$

where the same distance is now measured from the origin for the *f* function. The loading/unloading distinction is made based upon associated unit vectors prescribed on the loading surface by a vector operation as: $\widehat{n} : d\widehat{\sigma} > 0$ for loading, $\widehat{n} : d\widehat{\sigma} < 0$ for unloading, and $\widehat{n} : d\widehat{\sigma} = 0$ for neutral loading. Here, the unit vector, $\widehat{n}$ on $f = 0$, shows the loading direction defined as:

$$\widehat{n} = \frac{\partial f}{\partial \widehat{\sigma}} \Big/ \left(\frac{\partial f}{\partial \widehat{\sigma}} \frac{\partial f}{\partial \widehat{\sigma}}\right)^{1/2} \tag{7}$$

The above is valid only for hardening materials and is changed in the case of softening behavior with the introduction of $d\sigma^e$ calculated using elastic strains. That is, a slightly more complex relationship should be used for loading and unloading (see Mroz and Zienkiewicz[52]), such that the sign of $\widehat{n} : d\sigma^e$ gives the correct direction where:

$$d\sigma^e = D^e d\varepsilon \tag{8}$$

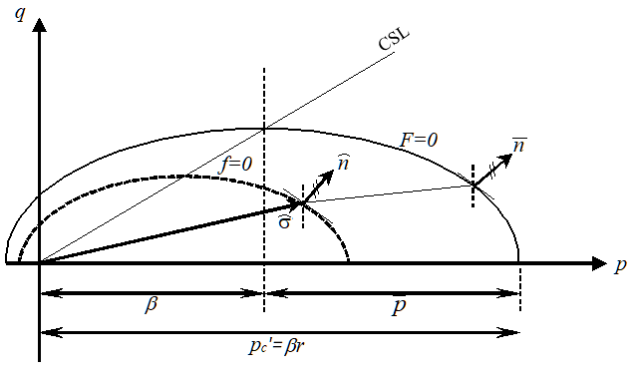

Figure 1. Loading and bounding surfaces.

2.1.2. Stress-Strain Relationship and Plastic Strains

Decomposition of strains is written incrementally using classical plasticity as,

$$d\varepsilon_{ij} = d\varepsilon_{ij}^{e} + d\varepsilon_{ij}^{p} \tag{9}$$

where the elastic and plastic strains are calculated individually as,

$$d\varepsilon_{ij}{}^{e} = C_{ijkl}^{e} d\sigma_{kl}^{'} \tag{10}$$

$$d\varepsilon_{ij}{}^{p} = \frac{1}{H_{L/U}} \left[n_{g}^{L/U} \otimes \widehat{n} \right] : d\sigma_{ij}^{'} \tag{11}$$

Here C_{ijkl}^{e} is the inverse elastic matrix, and $H_{L/U}$ is the elastic modulus, which should be defined in loading (L) or unloading (U). With the help of the consistency condition, the elastoplastic constitutive matrix, D^{ep}, is evaluated. Although the plastic flow direction and the direction of the stress vector could be selected differently through a plastic potential function, $g(\sigma)$, in this study, for simplicity, an associated flow rule is employed without giving up much of the accuracy of the yielding, $n_g = \widehat{n} = n$. Effective stress increments, $d\sigma_{ij}^{'}$ are calculated through the stress-strain relationship as,

$$d\sigma_{ij}^{'} = D_{ijkl}^{ep} d\varepsilon_{kl} \tag{12}$$

where D_{ijkl}^{ep} is in matrix form, and $d\varepsilon_{kl}$ is the strain increment. Carrying out the usual steps of derivation through the consistency condition, we have the following written in the particular order leading ultimately to the material matrix,

$$d\varepsilon^{p} = d\lambda \frac{\partial F}{\partial \sigma} \tag{13}$$

$$d\sigma' = D^{e} \left[\varepsilon - d\lambda \frac{\partial F}{\partial \sigma} \right] \tag{14}$$

$$dF = \frac{\partial F}{\partial \sigma} d\sigma + \frac{\partial F}{\partial p_c} \frac{\partial p_c}{\partial \varepsilon_p} d\varepsilon_p = 0 \tag{15}$$

Here (13) and (14) are used in (15), giving the plastic strain slip rate as:

$$d\lambda = \left[\frac{\partial F^{T}}{\partial \sigma} D^{e} \Big/ \left(\frac{\partial F^{T}}{\partial \sigma} D^{e} \frac{\partial F}{\partial \sigma} + H \right) \right] d\varepsilon \tag{16}$$

which, when used back in (14) yields:

$$D^{ep} = D^{e} \left[I - \frac{\left(\frac{\partial F}{\partial \sigma} \frac{\partial F}{\partial \sigma}^{T} D^{e} \right)}{\left(\frac{\partial F}{\partial \sigma}^{T} D^{e} \frac{\partial F}{\partial \sigma} + H \right)} \right] \tag{17}$$

Here the plastic modulus is $H = H_{L/U}$ depending upon loading (L) or unloading (U). It is self-evident that,

$$D^{ep} = \left[D^{e} - \frac{\left(D^{e} n_{L/U}\, n^{T} D^{e} \right)}{\left(n^{T}\, D^{e}\, n_{L/U} + H_{L/U} \right)} \right] \tag{18}$$

where

$$n = \frac{\frac{\partial F}{\partial \sigma}}{\left(\frac{\partial F}{\partial \sigma} \frac{\partial F}{\partial \sigma} \right)^{½}} \tag{19}$$

The soil's elastic shear and bulk moduli, G_e, and K_e depend on mean effective stress. Thereby:

$$d\varepsilon_{s}^{e} = \frac{dq}{G_e}, G_e = G_0 \frac{p^{'}}{p_0} \tag{20}$$

$$d\varepsilon_{v}^{e} = \frac{dp^{'}}{K_e}, K_s = K_0 \frac{p^{'}}{P_0} \tag{21}$$

are written with G_0 and K_0 as their initial values and p_0 as the reference pressure.

2.1.3. Proposed Hardening Law

The evolution of strain-hardening behavior is achieved by updating the hardening parameter p_c. Along with this, an interpolation rule considering the location of the current stress vector on the loading surface, $\overline{\sigma}$ in relation to the location of the corresponding stress vector on the bounding surface, $\overline{\sigma}$ (**Figure 1**), is introduced. In this study, a new hardening rule, along with a new local degradation function through a model parameter γ, to evaluate the plastic hardening modulus, is proposed. The following form of such a function is adopted using volumetric plastic strain as a dependent variable as:

$$X = m(r) \left(\frac{p_c}{100} \right) \left(\frac{1}{\widehat{\sigma}_{m}^{'}} \right) \tag{22}$$

where p_c is in *kPa* unit and updated using the following function,

$$p_c = p_0 \exp\left(-\mu_0 \varepsilon_{\nu}^{p} \right) \tag{23}$$

where

$$\mu_0 = \frac{1 + e_0}{\lambda - \kappa} \tag{24}$$

with e_0 as the initial void ratio and λ, κ being the loading and unloading slopes of the compression behavior about the critical state theory, ε_v^p is the total volumetric plastic strain. In Equation (22), $\widehat{\sigma}_m^{'}$ is the current mean effective stress on the loading surface, and *m(r)* is a function of *r*, the ratio of the diameter of the ellipse (i.e., p_c of a given *F* function) to the distance of the center measured from the origin. So, a definition of the stress vector inside the bounding surface is included in determining the ratios of stresses, *X*. Such a form is proposed for *m* as:

$$m(r) = c_0 + c_1 M_c \tag{25}$$

whose coefficients, c_0 and c_1, are determined either as a function of *r* or taken simply as constants for a specific experimental simulation. In this study, we seek a simple relation between *X* and the slope M_c, as in (25), which we find varies linearly to capture the soil response and is also a function of the *r* value (see **Figure 2**). While $r \geq 2$ is mostly applicable except for large values of *r*; for $r = 2$, *X* can also be determined directly by solving $F = 0$ equation for the stress vector, $\bar{\sigma}$on the bounding surface. Also, the range $2 < r < 3$ varies as much as $r \geq 3$, and this study distinguishes between them. The plastic modulus now becomes:

$$H_L = H_{cs} X^{\gamma} \tag{26}$$

where γ varies with the accumulated deviatoric plastic strain, ε_S^p, through an exponential function as:

$$\gamma = \gamma_0 \exp\left(-D\varepsilon_s^p\right) \tag{27}$$

where γ_0 and *D* are the additional model parameters and:

$$\varepsilon_s^p = \int \sqrt{\frac{2}{3} d\varepsilon_s^p d\varepsilon_s^p} \tag{28}$$

$$d\varepsilon_s^p = d\varepsilon_{ij}^p - \delta_{ij}\, d\varepsilon_v^p/3 \tag{29}$$

Also, H_{cs} in (26) is the critical state value of the plastic modulus calculated using the following,

$$H_{cs} = -\frac{\frac{\partial F}{\partial \varepsilon_v^p}\left(\frac{\partial F}{\partial \sigma_m}\right)}{\left(\frac{\partial F}{\partial \sigma}\right)^T \left(\frac{\partial F}{\partial \sigma}\right)} \tag{30}$$

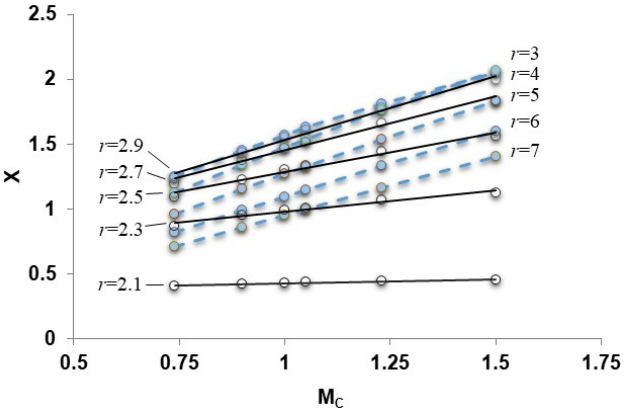

Figure 2. Variations of X with M_c for various *r*.

This method of defining the plastic modulus produces relatively successful results, particularly for clay-like cohesive soils. The γ controls the degradation of the plastic modulus H_L, essentially controlling how close it is to its critical value H_{cs}. While the parameter γ_0 is the initial value of γ signifying the starting point of X, the parameter *D* controls the curvature of degradation, which determines how fast the soil will reach failure through plastic strain accumulation. The presented formulation is used to simulate several triaxial compression tests.

2.1.4. Elastic Response

Elastic strains are calculated using the initial values of elastic moduli, which evolve during loading depending upon the change in effective mean stress. To understand the effect of nonlinear elastic behavior in terms of pressure dependency of elastic moduli on the sandy soil response, the study of Tatlıoğlu et al.[53] employs several nonlinear elastic behaviors associated with the variations of elastic bulk modulus, *K*, and shear modulus *G*. Based on their results, the following relationships are also employed in this study:

$$d\varepsilon_s^e = \frac{1}{G} = \frac{p_r}{p' G_0} d\sigma_s \tag{31}$$

$$d\,\varepsilon_\nu^e = \frac{1}{K} = \frac{p_r}{p' K_0} d\,\sigma_\nu \tag{32}$$

The proposed model consists of several parameters: some are soil physical properties, while others are associated with model calibration. The parameters, G_0, K_0, are the initial shear modulus and bulk modulus, respectively; initial void ratio is e_0; the stress ratios of compression and extension sides are M_c and M_e; the radius of the yield surface is *r*; the model parameters are c_0, c_1, H_0, γ_0, *D*; the

slopes of compression are λ, κ, and the initial value of pre-consolidation stress is p_{c0}. These parameters can be easily determined from a series of triaxial compression tests on a specific soil sample. In light of other similar models, the yield surface parameter r, as well as the coefficients c_0 and c_1, which are defined through an additional function in the hardening law, provide further support for the proposed model. These parameters are sufficient for the current model to accurately capture the cohesive soils' monotonic and cyclic behavior, compared with other bounding surface models.

3. Simulation of Triaxial Compression Tests

The preceding formulation is implemented in a computer program and verified with available tests, whose simulations are presented to demonstrate the model's capability. Equation (14), which now employs (18), is computed using the relationship in (12), which is now rewritten as:

$$(\Delta\sigma)_{n+1}^{i+1} = (D^{ep})_{n+1}^{i+1}\,(\Delta\varepsilon)_{n+1}^{i+1} \tag{33}$$

where '*n*' is the load increment and '*i*' is the iteration number. In this study, the integration of the necessary constitutive equations is carried out using the fully explicit integration scheme requiring the previously converged stresses, σ_n, strains ε_n, as well as the hardening and related parameters, $(H_L)_n$, $(\varepsilon_s^p)_n$, $(\varepsilon_v^p)_n$, $(X)_n$ and γ_n to update the current values of the same variables with 'n+1' subscript. Hence, a direct integration procedure is employed in the computational scheme, where Equations (13) through (19) are computed in the given order to calculate the D^{ep} matrix of (33). In this explicit integration procedure, Equation (22) through (25) are sequentially computed to integrate Equation (26) into (18).

3.1. Monotonic Loading Tests

Drained and undrained triaxial compression tests are simulated on normally consolidated (NC) and over-consolidated (OC) clays under stress and strain-controlled loadings. **Figure 3** shows NC undrained clay simulation results in a monotonic drained test, which is used in calibrating the model parameters. Model results match the test results of Balasubramaniam and Chaudhry[54], particularly in the stress-strain relationship and stress-path behavior, although there is an average error amount of about 3% in the mean stress behavior. Pore pressure variation captures the initial and residual response qualitatively along with the actual trend.

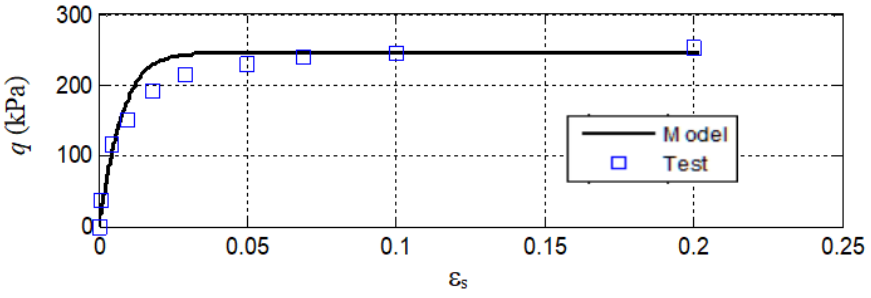

(**a**)

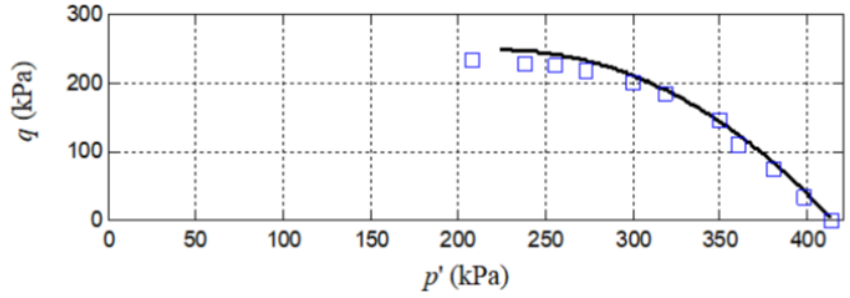

(**b**)

Figure 3. *Cont.*

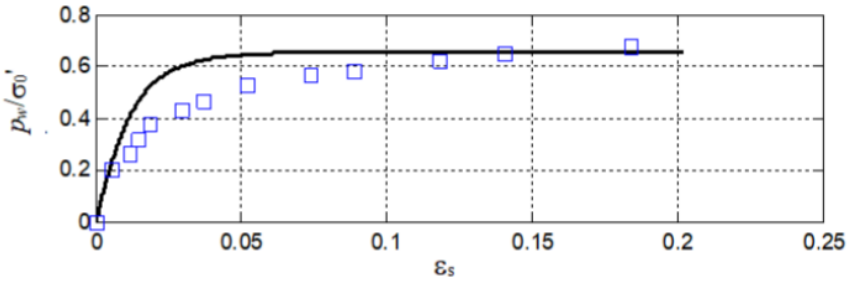

(**c**)

Figure 3. Constant mean stress triaxial undrained test simulations of NC Bangkok clay, (**a**) Deviatoric stress-strain relationship, (**b**) Stress path, (**c**) Pore pressure-strain relationship.

The following test data are used in predicting the monotonic behavior of clay soils based on the calibration process of the parameters given in **Table 1** as mentioned.

Table 1. Model parameters of static triaxial test simulations.

Figure No.	G_0 (kPa)	K_0 (kPa)	p_{c0} (kPa)	M	H_0	r	D	γ_0
Figures 3–4	12,420	15,000	414	1.1	6.6	2.0	100–150	10
Figures 5–6	5280	5510	414	0.9	165	2.1	100	10

Another test used to verify the current formulation is the constant mean stress-triaxial drained test of the same Bangkok clay, as shown in **Figure 4**. The stress ratio-strain relationships are presented, where the overall drained behavior is successfully captured, particularly in terms of shear behavior. Volumetric response is slightly underpredicted (showing a higher maximum discrepancy at a single location with an average value of 5%) compared to the experimentally measured behavior.

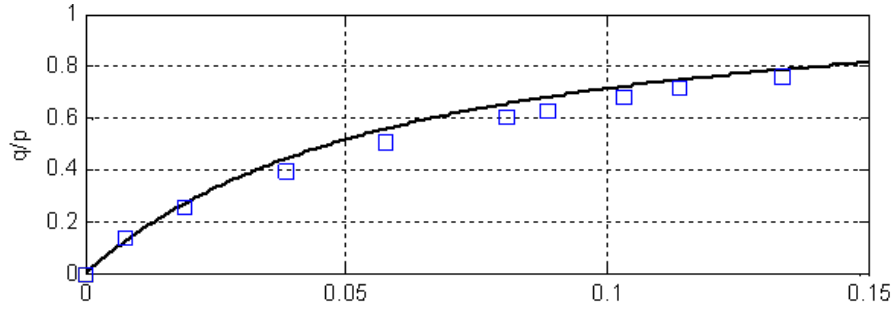

(**a**)

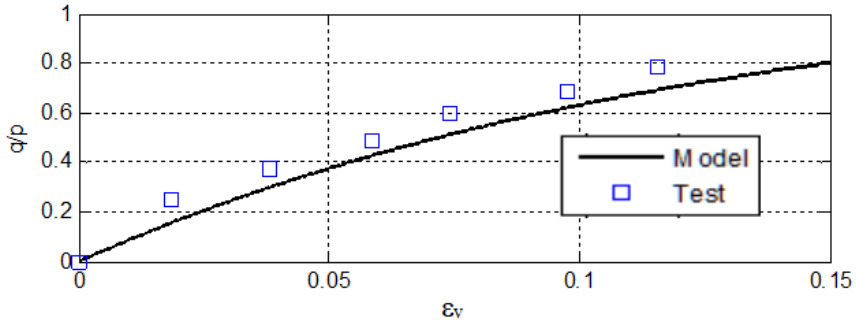

(**b**)

Figure 4. Constant σ_3' drained triaxial test simulation of NC Bangkok clay, (**a**) Stress ratio-shear strain relationship, (**b**) Stress ratio-volumetric strain relationship.

Figure 5 presents the drained triaxial simulation of the tests on NC clay[55]. The volumetric behavior is captured more accurately with less amount of maximum error in the drained case, including the stress-strain relationship. The current formulation captures both volumetric strain-axial strain and deviatoric stress-axial strain relationships.

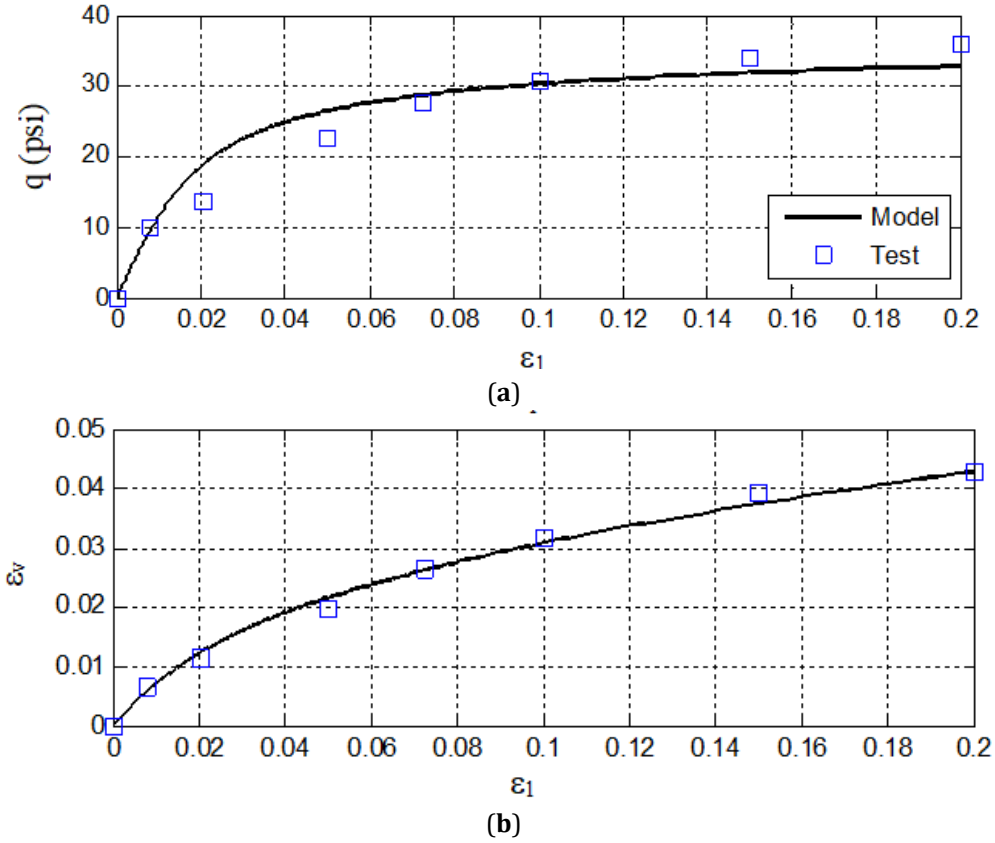

Figure 5. Drained triaxial response of NC clay, (**a**) Deviatoric stress-axial strain relationship, (**b**) Volumetric strain-axial strain relationship.

Another monotonic test simulated is a highly OC clay given in **Figure 6** under constant mean effective stress[55]. This prediction is significant in that it presents the robustness of the proposed model and its implementation in the case of a high OC clay. Pore pressure response is captured reasonably well, with a slight discrepancy in the amount of axial strain required to switch from compression to tension.

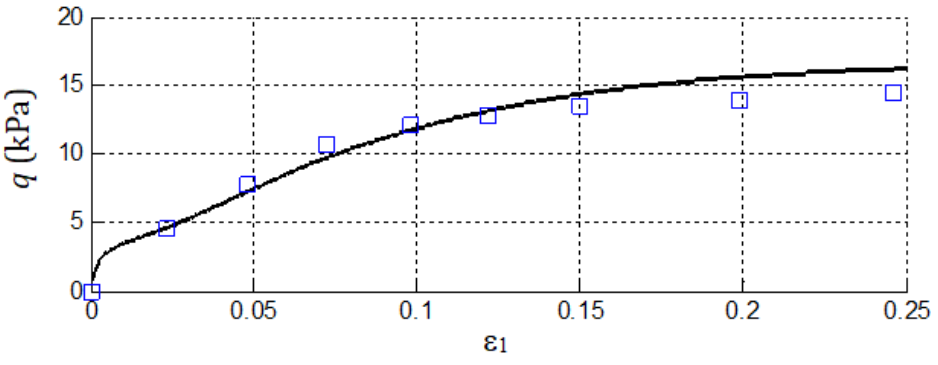

Figure 6. *Cont.*

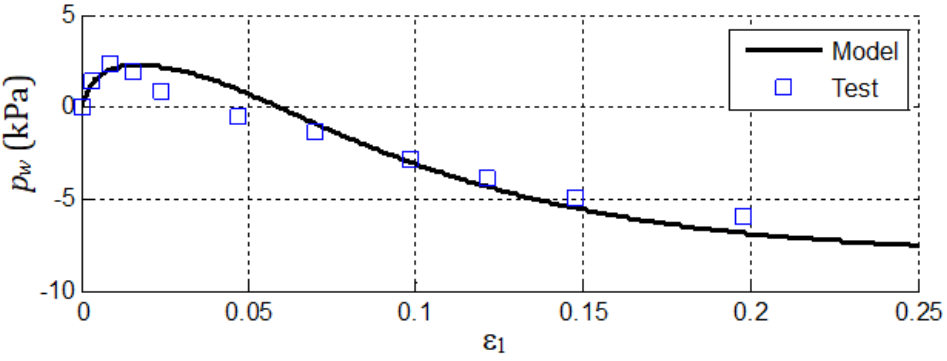

(**b**)

Figure 6. Constant σ_3' triaxial simulations of undrained OC clay, OCR = 24, (**a**) Deviatoric stress-axial strain relationship, (**b**) Pore pressure-axial strain relationship.

3.2. Cyclic Loading Tests

Cyclic undrained triaxial tests of NC clays are modeled in this section. G is either taken as a constant or as in (14) in the analyses. For the bulk modulus, the following relationship is employed:

$$K = (1 + e_0)\, p'/\kappa \tag{34}$$

Figure 7 shows the strain-controlled test as predicted by the simulation performed in this study using the proposed hardening rule. Results, given in terms of stress-strain relationship, stress path, and pore water pressure generation are well simulated. They are all compared to the test results of Taylor and Bacchus[56] and predictions of the Generalized Plasticity Model by Zienkiewicz et al.[17], who used the following simple interpolation rule for the plastic modulus:

$$H_L = H_{bs}(\delta/\delta_0)^{\gamma} \tag{35}$$

where H_{bs} is the value of the plastic modulus on the bounding surface, δ_0 is the distance from the origin to the image stress on bounding surface, δ is the distance of current stress from the origin. The parameter γ is taken here as in (27). Under a cyclic deviatoric strain of ε_q = ± 0.8%, a predictable response is obtained, where the effect of γ_0 as used in (35) in terms of providing a sensitivity analysis is also presented. The analyses well capture that the pore pressure build-up remains limited, leading to a limited decrease in the deviatoric stress (see **Figure 7a**). The difference between the previous analyses and predicted results is about 5% average. Analyses' parameters are shown in **Table 1**.

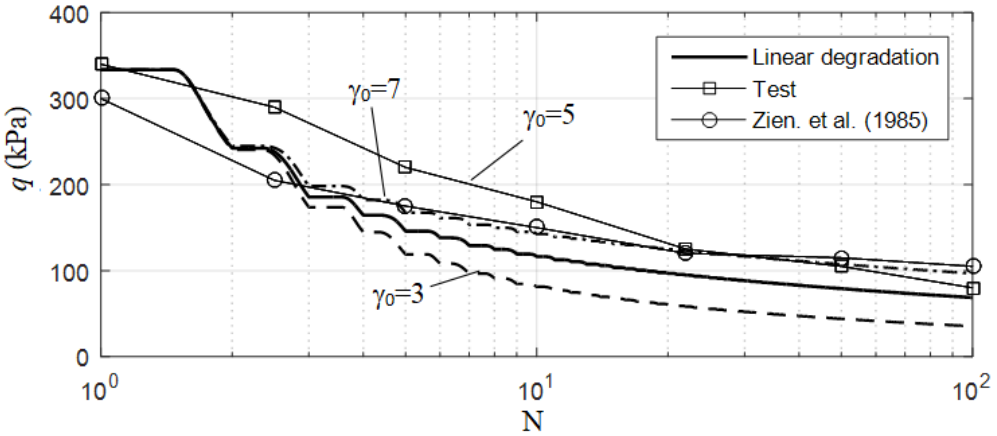

(**a**)

Figure 7. *Cont.*

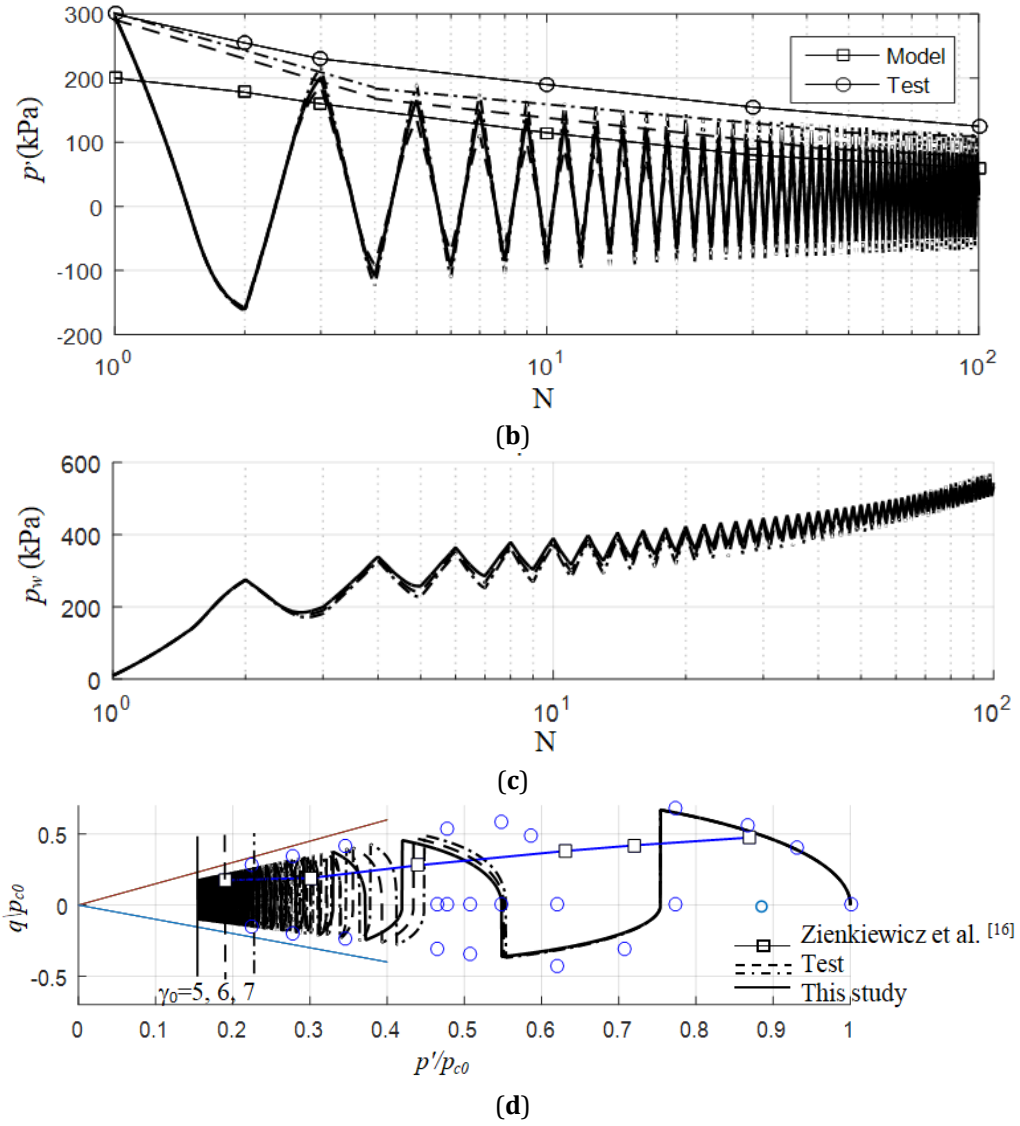

Figure 7. Cyclic strain-controlled undrained triaxial test simulation of NC clay, (**a**) Deviatoric stress, (**b**) Mean effective stress, (**c**) Pore pressure vs. N, (**d**) Stress path for various γ, p_{c0} = 300 kPa.

Figure 8 presents the pore pressure behavior of a soil fill, where the new interpolation rule with a constant is tested with the test data of Seed et al.[57], which is also compared with the prediction of the Generalized Plasticity Model by Zienkiewicz et al.[17], measured in the first ten loading cycles. The simulation of this study gives a good match with the tests[57], where, depending on the value of *D*, the difference becomes about 3–5%. As the loading continues, however, the response is captured more accurately by a linear relationship of degradation employing the parameter *D*.

Another simulation is performed on the cyclic triaxial test results as performed by Taylor and Bacchus[56]. Strain-controlled simulations of clay, presented in terms of stress path, pore pressure, and mean effective stress variations for p_{c0} = 442 kPa of initial consolidation stress, are simulated in **Figure 9**. While the reduction in mean effective stress is predicted well, including the stress path variation, the pore pressure response is over-predicted towards the end of the load cycles. Simulation of a strain-controlled two-way loading test of Kuntsche[58] on NC kaolin clay can be seen in **Figure 10**. The hysteretic behavior and reduction in effective stress leading to cyclic mobility are captured fairly well with the new proposed hardening rule. In contrast to the previous test in **Figure 9**, the stress path response is captured with less success here through the ongoing cycles of loading with some underprediction except for the initial static response and

the final prediction of the deviatoric stress ratio, which are evaluated accurately. The root mean square error of **Figure 10** is calculated to vary between 0.02 and 0.88. **Figure 10** also shows the hysteretic cyclic-stress strain relationship, which is captured by the proposed model for this cohesive soil as well.

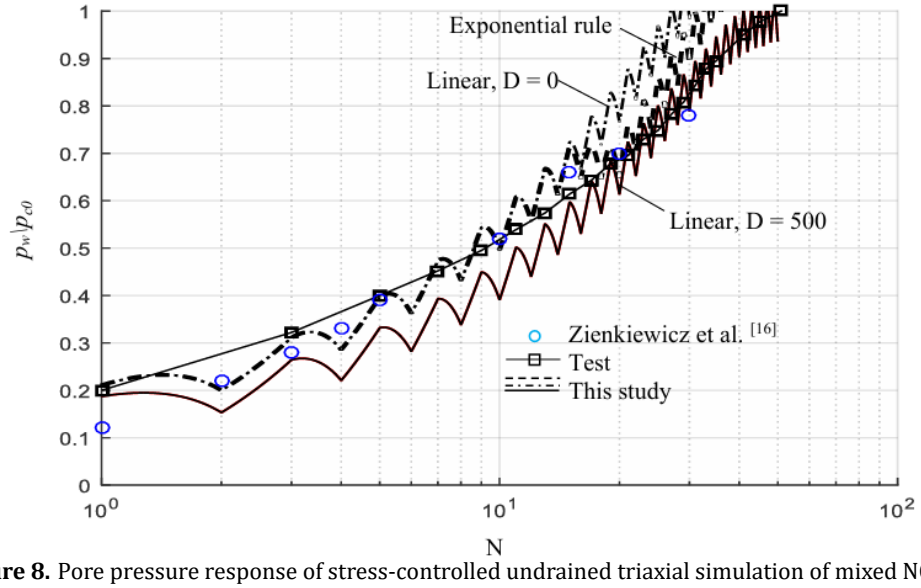

Figure 8. Pore pressure response of stress-controlled undrained triaxial simulation of mixed NC fill.

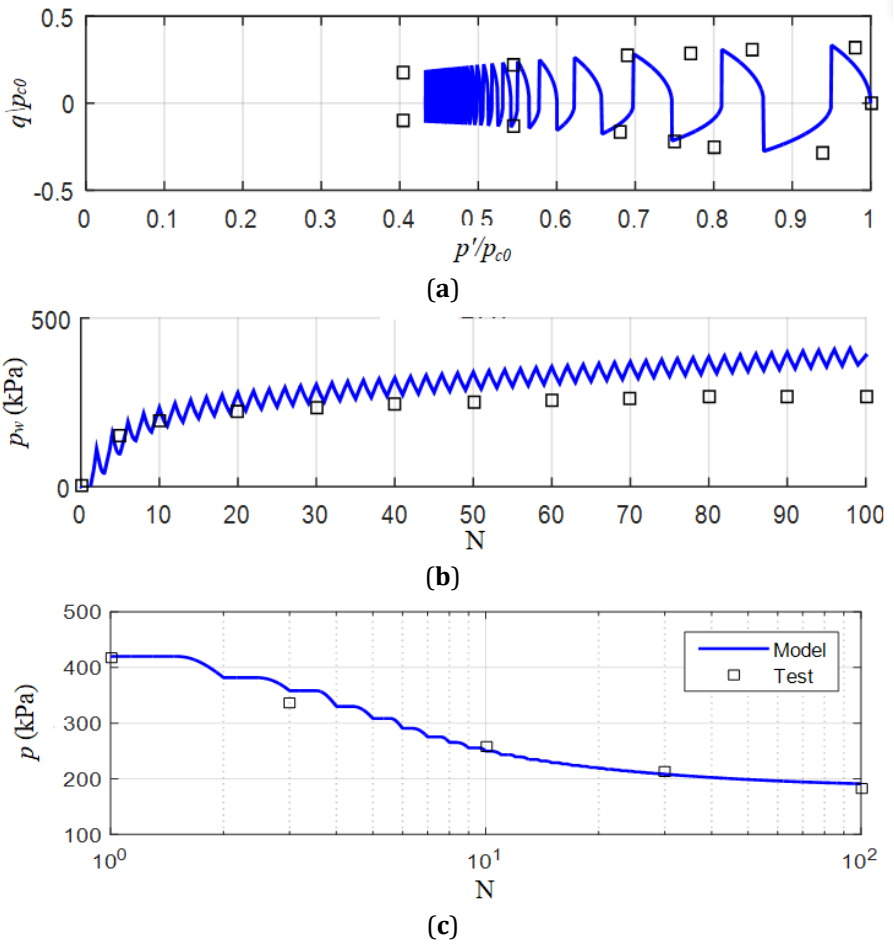

Figure 9. Strain-controlled undrained triaxial simulations of NC clay, (**a**) Stress path, (**b**) Pore pressure, (**c**) Mean effective stress variation, p_{c0} = 442 kPa.

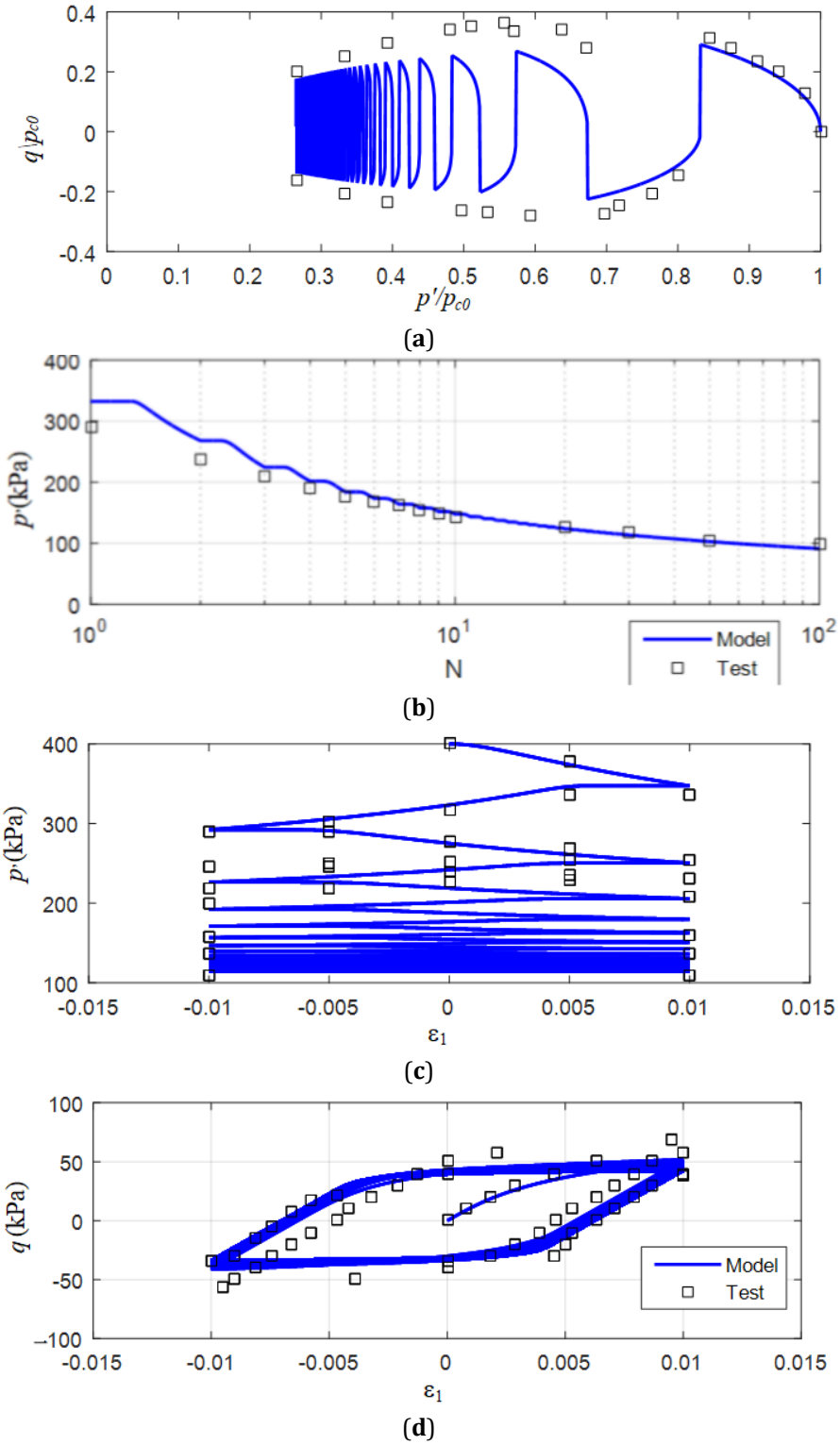

Figure 10. Two-way strain-controlled undrained triaxial test simulation of NC kaolin, (**a**) Stress path, (**b**) Mean effective stress, (**c**) Mean effective stress-axial strain, (**d**) Deviatoric stress-axial strain relationship, p_{c0} = 400 kPa.

Another comparison was made using a fairly new set of data by Duque et al.[59] on Malaysian kaolin for various cyclic stress ratios (CSR) and number of load cycles, N_f. **Figure 11a–f** show the test data and its calibrated model developed with the proposed model. The response under monotonic loading was analyzed by means

of undrained monotonic triaxial experiments with different initial mean effective stresses and overconsolidation ratios. Stress path responses are very well captured by the proposed hardening law of the kaolin clay under undrained cyclic triaxial tests. The percent error is obtained to be less than 1%. **Figure 11a,c,e** give the results of the calibrated test data via the proposed model while **Figure 11b,d,f** present the cyclic undrained triaxial test data.

According to the experimental study of Duque et al.[59] on Malaysian kaolin clay, it is suggested that a drastic increase in the accumulation rate of vertical strains and pore water pressures with increasing deviatoric stress amplitudes are obtained. The simulation results of this study match fairly well with the experimental data given in **Figure 11**. While the stress path response goes until about 100 kPa of mean effective stress before failure as in **Figure 11a,c,e** show more resilient behavior until about 20–30 kPa of residual mean effective stress is left in the soil. The stress-controlled cyclic shearing behavior obtained in these cyclic triaxial experiments led to a significant amount of stress softening prior to failure of the soil samples. **Table 2** shows the parameters used in the cyclic triaxial test simulations.

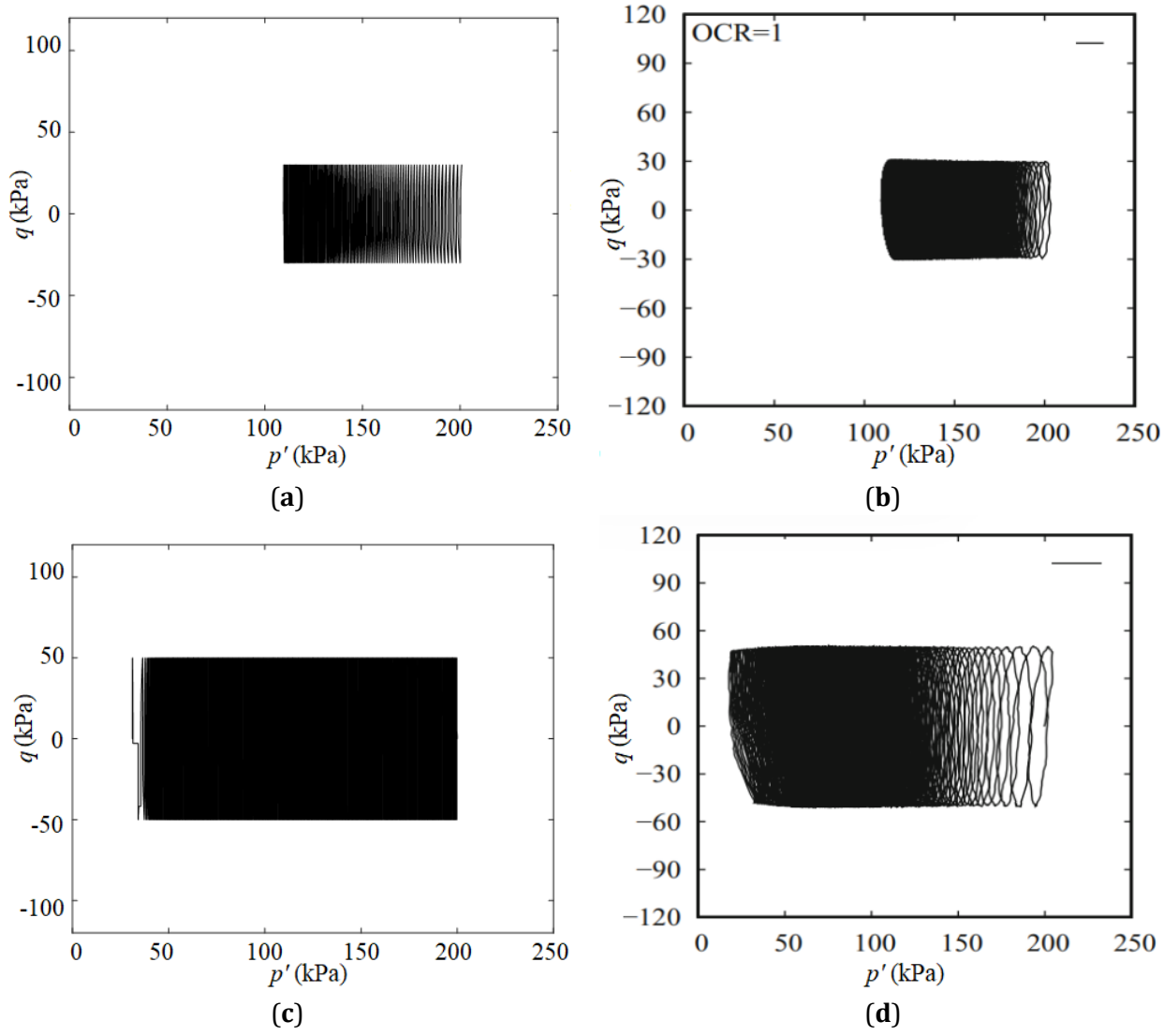

Figure 11. *Cont.*

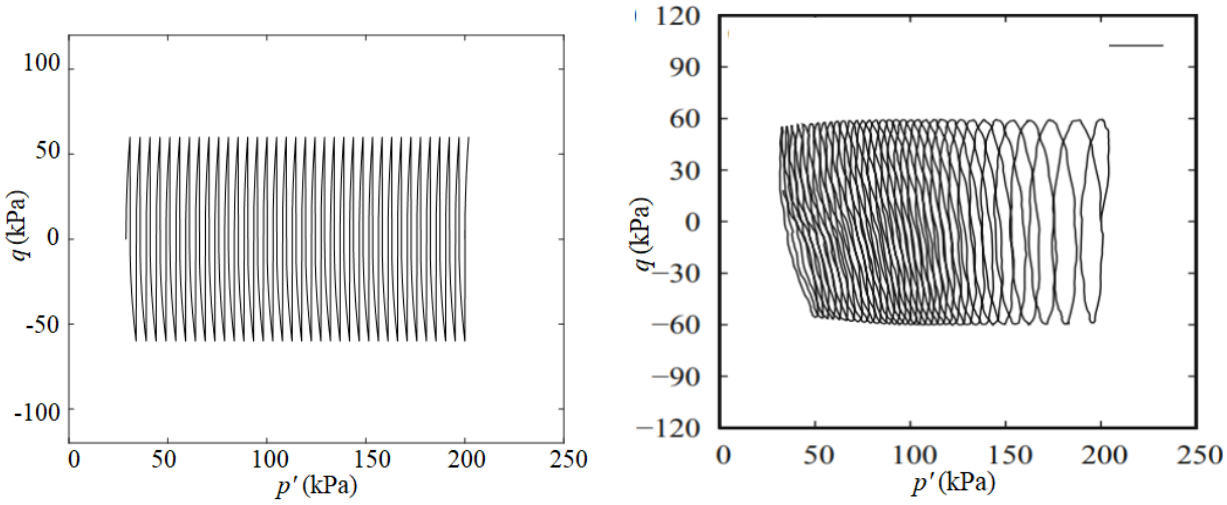

(e) **(f)**

Figure 11. Modeling cyclic undrained response of Malaysian clay in terms of stress paths; (**a**,**b**) CSR = 0.075, N_f > 5000; (**c**,**d**) CSR = 0.125, N_f = 343; (**e**,**f**) CSR = 0.150, N_f = 36; (**a**,**c**,**e**) Model predictions; (**b**,**d**,**f**) Duque et al.[59] experiments, OCR = 1.

Table 2. Model parameters of cyclic triaxial test simulations.

Figure No.	G_0 (kPa)	K_0 (kPa)	r	e_0	M_c	M_e	γ_0	D	λ	κ	p_{c0} (kPa)
Figure 7	17,300	-	2.0	0.962	1.5	1.0	10	100	0.132	0.021	442
Figure 8	25,000	34,000	2.3–2.5	-	1.5	1.0	10	0–500	0.1	0.005	103
Figure 9	17,300	-	2.0	0.962	1.5	1.0	17.5	100	0.132	0.021	442
Figure 10	8000	-	2.0	0.962	0.74	0.6	20	100	0.2	0.05	400
Figure 11a	5500	11,900	2.02	1.327	1.23	1.0	8.0	100	0.04	0.042	200
Figure 11c	5500	11,900	2.02	1.340	1.23	1.0	8.4	100	0.41	0.042	200
Figure 11e	5500	11,900	2.02	1.311	1.23	1.0	8.4	100	0.51	0.035	200

4. Discussion

In this study, a novel hardening law proposed to capture the monotonic and cyclic behavior of clay-like cohesive seabed soils is presented. It is implemented with a novel formulation and integrated into the Bounding Surface Theory. An associated flow rule is used to simplify the formulation, in which the rate effects and soil anisotropy are not included. This can be considered a limitation for the proposed study. On the other hand, the developed hardening law requires only two additional model parameters to be calibrated to capture the monotonic and cyclic response of clay soil. The monotonic loading behavior of the clay is modeled with fairly good accuracy, with an average error of about 3% in the magnitudes of the response results. Cyclic loading-induced behaviors of cohesive soils are also captured fairly accurately by the proposed model, as shown by the stress-strain relationships, stress path responses, and pore pressure time histories. While about the same amount of error is obtained in the majority of analyses, some results indicate slightly larger error margins; however, the general trend is still accurately captured. Overall, the proposed study presents a novel hardening law for cohesive soils implemented within a bounding surface model. The proposed model, whose mathematical formulation is more practical and simpler than that of other similar models for the same type of soil, is integrated into a computer program that uses an explicit numerical scheme. The proposed model can be used to solve ocean, coastal, and offshore geotechnical engineering problems, including the response to a large number of stress cycles with fairly high accuracy.

5. Conclusions

In this paper, the constitutive behavior of cohesive seabed soils, in particular clays, under monotonic and cyclic loading is studied. A more effective, straightforward, yet novel hardening law, along with a new inter-

polation function, is proposed to evaluate the plastic hardening modulus associated with accumulated plastic strains. The related theoretical relations are developed and incorporated into a Bounding Surface Plasticity framework. The proposed model's mathematical formulation is more practical and simpler than those of similar models for cohesive seabed soils. It is integrated into a computer program through an explicit numerical scheme. Then the constitutive behavior under monotonic and cyclic loadings, including the stress-strain relationship, stress path, volumetric strain responses in drained tests, and corresponding pore pressure-time histories in undrained tests, is evaluated. Predictions are verified using monotonic and cyclic tests for both NC and OC clays to ensure rigorous model validation. Results indicate that the proposed model matches well with the available tests, yielding results that not only capture the main features of the constitutive behavior of seabed clays but also do so through a simple hardening law. That is, the proposed model leverages the simplification and sophistication introduced into its theory, as demonstrated in this study.

Funding

This was partially funded by the Istanbul Technical University Research Projects Unit (BAP) with project number 37606.

Institutional Review Board Statement

Not applicable.

Informed Consent Statement

Not applicable.

Data Availability Statement

The data that support the findings of this study are available on request from the corresponding author. The data are not publicly available due to privacy or ethical restrictions.

Acknowledgments

The author would like to acknowledge the partial financial support of Istanbul Technical University Research Projects Unit (BAP) with project number 37606. The support from ITU is highly appreciated.

Conflicts of Interest

The authors declare no conflict of interest.

References

[1] Mroz, Z., 1967. On the Description of Anisotropic Work-Hardening. Journal of the Mechanics and Physics of Solids. 15(3), 163–175. DOI: https://doi.org/10.1016/0022-5096(67)90030-0

[2] Prevost, J.-H., 1977. Mathematical Modeling of Monotonic and Cyclic Undrained Clay Behavior. International Journal for Numerical and Analytical Methods in Geomechanics. 1(2), 195–216. DOI: https://doi.org/10.1002/nag.1610010206

[3] Mroz, Z., Norris, V.A., Zienkiewicz, O.C., 1978. An Anisotropic Hardening Model for Soils and Its Application to Cyclic Loading. International Journal for Numerical and Analytical Methods in Geomechanics. 2(3), 203–221. DOI: https://doi.org/10.1002/nag.1610020303

[4] Mroz, Z., Norris, V.A., Zienkiewicz, O.C., 1981. An Anisotropic Critical State Model for Soils Subject to Cyclic Loading. Géotechnique. 31(4), 451–469. DOI: https://doi.org/10.1680/geot.1981.31.4.451

[5] Hirai, H., 1987. An Elastoplastic Constitutive Model for Cyclic Behavior of Sands. International Journal for Numerical and Analytical Methods in Geomechanics. 11(5), 503–520. DOI: https://doi.org/10.1002/nag.1610110506

[6] Krieg, R.D., 1975. A Practical Two Surface Plasticity Theory. Journal of Applied Mechanics. 42(3), 641–646. DOI: https://doi.org/10.1115/1.3423656

[7] Dafalias, Y.F., Popov, E.P., 1975. A Model of Nonlinearly Hardening Materials for Complex Loading. Acta Mechanica. 21, 173–192. DOI: https://doi.org/10.1007/BF01181053

[8] Dafalias, Y.F., Hermann, L.R., 1982. Bounding Surface Formulation of Soil Plasticity. In: Pande, G.N., Zienkiewicz, O.C. (Eds.). Soil Mechanics—Transient and Cyclic Loads. Wiley & Sons: Chichester, UK. pp. 253–282.

[9] Dafalias, Y.F., 1986. Bounding Surface Plasticity I: Mathematical Foundation and Hypoplasticity. Journal of Engineering Mechanics ASCE. 112(9), 966–

987. DOI: https://doi.org/10.1061/(ASCE)0733-9399(1986)112:9(966)

[10] Kaliakan, V.N., Dafalias, Y.F., 1989. Simplifications to the Bounding Surface Model for Cohesive Soils. International Journal for Numerical and Analytical Methods in Geomechanics. 13(1), 91–100. DOI: https://doi.org/10.1002/nag.1610130108

[11] Wang, Z.L., Dafalias, Y.F., 1990. Bounding Surface Hypoplasticity Model for Sand. Journal of Engineering Mechanics ASCE. 116(5), 983–1001. DOI: https://doi.org/10.1061/(ASCE)0733-9399(1990)116:5(983)

[12] Pietruszczak, S., Poorooshasb, H.B., 1985. Modeling of Liquefaction and Cyclic Mobility Effects in Sand. In Proceedings of the 5th International Conference on Numerical Methods in Geomechanics, Nagoya, Japan, 1–5 April 1985; pp. 1867–1875.

[13] Poorooshasb, H.B., Pietruszczak, S., 1985. On Yielding and Flow of Sand: A Generalized Two Surface Model. Computers and Geotechnics. 1(1), 33–58. DOI: https://doi.org/10.1016/0266-352X(85)90014-X

[14] Poorooshasb, H.B., Pietruszczak, S.A., 1986. Generalized Flow Theory for Sand. Soils and Foundations. 26(2), 1–15. DOI: https://doi.org/10.3208/sandf1972.26.2_1

[15] Zienkiewicz, O.C., Mroz, Z., 1984. Generalized Plasticity Formulation and Application to Geomechanics. In: Desai, C.S., Gallagher, R.H. (Eds.). Mechanics of Engineering Materials. Wiley: New York, NY, USA. pp. 655–679.

[16] Poorooshasb H.B., Yang Q.S., Clark J.I., 1990. Nonlinear Analysis of a Seabed Deposit Subjected to the Action of Standing Waves. Mathematical and Computer Modelling. 13(4), 45–58.

[17] Zienkiewicz, O.C., Leung, K.H., Pastor, M., 1985. Simple Model for Transient Soil Loading in Earthquake Analysis. International Journal for Numerical and Analytical Methods in Geomechanics. 9(5), 477–498. DOI: https://doi.org/10.1002/nag.1610090505

[18] Pastor, M., Zienkiewicz, O.C., Chan, A.H.C., 1990. Generalized Plasticity and Modeling of Soil Behavior. International Journal for Numerical and Analytical Methods in Geomechanics. 14(3), 151–190. DOI: https://doi.org/10.1002/nag.1610140302

[19] Yao, Y.P., Gao, Z.W., Zhao, J.D., et al., 2012. Modified UH Model: Constitutive Modeling of Overconsolidated Clays Based on a Parabolic Hvorslev Envelope. Journal of Geotechnical and Geoenvironmental Engineering ASCE. 138(7), 860–868. DOI: https://doi.org/10.1061/(ASCE)GT.1943-5606.0000649

[20] Chen, B., Xu, Q., Sun, D., 2014. An Elastoplastic Model for Structured Clays. Geomechanics and Engineering. 7(2), 213–231. DOI: https://doi.org/10.12989/gae.2014.7.2.213

[21] Cheng, X., Wang, J., 2016. An Elastoplastic Bounding Surface Model for the Cyclic Undrained Behavior of Saturated Soft Clays. Geomechanics and Engineering. 11(3), 325–343. DOI: https://doi.org/10.12989/gae.2016.11.3.325

[22] Park, D.S., 2016. Rate of Softening and Sensitivity for Weakly Cemented Sensitive Clays. Geomechanics and Engineering. 10(6), 827–836. DOI: https://doi.org/10.12989/gae.2016.10.6.827

[23] Elia, G., Rouainia, M., 2016. Investigating the cyclic behavior of clays using a kinematic hardening soil model. Soil Dynamics and Earthquake Engineering. 88, 399–411. DOI: https://doi.org/10.1016/j.soildyn.2016.06.014

[24] Carlton, B.D., Pestana, J.M., 2016. A unified model for estimating the in-situ small strain shear modulus of clays, silts, sands, and gravels. Soil Dynamics and Earthquake Engineering. 88, 345–355. DOI: https://doi.org/10.1016/j.soildyn.2016.01.019

[25] Buchely, M.F., Maranon, A., Silberschmidt, V.V., 2016. Material model for modeling clay at high strain rates. International Journal of Impact Engineering. 90, 1–11. DOI: https://doi.org/10.1016/j.ijimpeng.2015.11.005

[26] Cuvilliez, S., Djouadi, I., Raude, S., et al., 2017. An elastoviscoplastic constitutive model for geomaterials: Application to hydromechanical modeling of claystone response to drifting excavation. Computers and Geotechnics. 85, 321–340. DOI: https://doi.org/10.1016/j.compgeo.2016.08.004

[27] Deng, Q.-L., Ren, X.-W., 2017. An energy method for deformation behavior of soft clay under cyclic loads based on dynamic response analysis. Soil Dynamics and Earthquake Engineering. 94, 75–82. DOI: https://doi.org/10.1016/j.soildyn.2016.12.012

[28] Luque, R., Bray, J.D., 2017. Dynamic analyses of two buildings founded on liquefiable soils during the Canterbury earthquake sequence. Journal of Geotechnical and Geoenvironmental Engineering. 143(9), 04017067. DOI: https://doi.org/10.1061/(ASCE)GT.1943-5606.0001736

[29] Hadidi, R., Dinsick, A., Wahl, D., et al., 2017. Characterization and seismic performance evaluation of Bouquet Canyon Dam No. 1. In Proceedings of the PBD-III Vancouver 2017: the 3rd International Conference on Performance Based Design in Earthquake Geotechnical Engineering, Vancouver, BC, Canada, 16–20 July 2017.

[30] Tasiopoulou, P., Giannakou, A., Chacko, J., de Wit, S., 2019. Liquefaction triggering and post-liquefaction deformation of laminated deposits. Soil Dynamics and Earthquake Engineering. 124,

330–344. DOI: https://doi.org/10.1016/j.soildyn.2018.04.044

[31] Schanz, T., Vermeer, P.A., Bonnier, P.G., 1999. The hardening-soil model: Formulation and verification. In: Brinkgreve, R.B.J. (Ed.). Beyond 2000 in Computational Geotechnics. Balkema: Rotterdam, Netherlands. pp. 281–290.

[32] Shi, Z., Finno, R.J., Buscarnera, G., 2018. A hybrid plastic flow rule for cyclically loaded clay. Computers and Geotechnics. 101, 65–79. DOI: https://doi.org/10.1016/j.compgeo.2018.04.018

[33] Yao, Y.-P., Liu, L., Luo, T., et al., 2019. Unified hardening (UH) model for clays and sands. Computers and Geotechnics. 110, 326–343. DOI: https://doi.org/10.1016/j.compgeo.2019.02.024

[34] Yang, M., Seidalinov, G., Taiebat, M., 2019. Multidirectional cyclic shearing of clays and sands: Evaluation of two bounding surface plasticity models. Soil Dynamics and Earthquake Engineering. 124, 230–258. DOI: https://doi.org/10.1016/j.soildyn.2018.05.012

[35] Boulanger, R.W., Ziotopoulou, K., 2019. A constitutive model for clays and plastic silts in plane-strain earthquake engineering applications. Soil Dynamics and Earthquake Engineering. 127, 105832. DOI: https://doi.org/10.1016/j.soildyn.2019.105832

[36] Wang, Y., Lei, J., Wang, Y., 2019. A post-cyclic strength degradation model for saturated soft clay. Ocean Engineering. 186, 106072. DOI: https://doi.org/10.1016/j.oceaneng.2019.05.054

[37] Zhao, Y., Lai, Y., Pei, W., et al., 2020. An anisotropic bounding surface elastoplastic constitutive model for frozen sulfate saline silty clay under cyclic loading. International Journal of Plasticity. 129, 1–32. DOI: https://doi.org/10.1016/j.ijplas.2020.102668

[38] Feng, D., Zhu, X., Wang, J., et al., 2020. The effects of cyclic loading on the reconsolidation behaviors of marine sedimentary clays under intermittent drainage conditions. Soil Dynamics and Earthquake Engineering. 106510. DOI: https://doi.org/10.1016/j.soildyn.2020.106510

[39] Cheng, X., Du, X., Lu, D., et al., 2020. A simple single bounding surface model for undrained cyclic behaviors of saturated clays and its numerical implementation. Soil Dynamics and Earthquake Engineering. 139, 106389. DOI: https://doi.org/10.1016/j.soildyn.2020.106389

[40] Cai, H., Zhang, Q., Ye, G., 2020. Numerical simulation on an undrained cyclic triaxial test of soft marine clay considering end restrictions of soil specimen. Ocean Engineering. 216, 108100. DOI: https://doi.org/10.1016/j.oceaneng.2020.108100

[41] Liu, Z., Xue, J., 2022. The deformation characteristics of a kaolin clay under intermittent cyclic loadings. Soil Dynamics and Earthquake Engineering. 153, 107112. DOI: https://doi.org/10.1016/j.soildyn.2021.107112

[42] Dafalias, Y.F., Manzari, M.T., Papadimitriou, A.G., 2006. SANICLAY: Simple anisotropic clay plasticity model. International Journal for Numerical and Analytical Methods in Geomechanics. 30(12), 1231–1257. DOI: https://doi.org/10.1002/nag.524

[43] Hu, C., Liu, H., 2015. A new bounding-surface plasticity model for cyclic behaviors of saturated clay. Communications in Nonlinear Science and Numerical Simulation. 22(1–3), 101–119. DOI: https://doi.org/10.1016/j.cnsns.2014.10.023

[44] Ni, J., Indraratna, B., Geng, X.-Y., et al., 2015. Model of soft soils under cyclic loading. International Journal of Geomechanics. 15(4), 04014095. DOI: https://doi.org/10.1061/(ASCE)GM.1943-5622.0000411

[45] Price, A.B., 2018. Cyclic strength and cone penetration resistance for mixtures of silica silt and kaolin. [PhD Thesis]. University of California, Davis, CA, USA.

[46] Boulanger, R.W., Price, A.B., Ziotopoulou, K., 2018. Constitutive modeling of the cyclic loading response of low plasticity fine-grained soils. In: Zhou, A., Tao, J., Gu, X., (Eds.). GeoShanghai International Conference. Springer: Singapore. pp. 1–13. DOI: https://doi.org/10.1007/978-981-13-0125-4_1

[47] Lu, D., Liang, J., Du, X., et al., 2019. Fractional elastoplastic constitutive model for soils based on a novel 3D fractional plastic flow rule. Computers and Geotechnics. 105, 277–290.

[48] Lu, D.C., Li, X.Q., Du, X.L., et al., 2019. A simple 3D elastoplastic constitutive model for soils based on the characteristic stress. Computers and Geotechnics. 109, 229–247.

[49] Liang, J., Lu, D., Du, X., et al., 2019. Non-orthogonal elastoplastic constitutive model for sand with dilatancy. Computers and Geotechnics. 118, 103329. DOI: https://doi.org/10.1016/j.compgeo.2019.103329

[50] Liang, J., Lu, D., Du, X., et al., 2022. A 3D non-orthogonal elastoplastic constitutive model for transversely isotropic soil. Acta Geotechnica. 17(1), 19–36.

[51] Bray, J.D., Boulanger, R.W., Cubrinovski, M., et al., 2017. PEER Report 2017/02: U.S.-New Zealand-Japan International Workshop: Liquefaction-Induced Ground Movements Effects. Pacific Earthquake Engineering Research Center: Berkeley, CA, USA.

[52] Mroz, Z., Zienkiewicz, O.C., 1984. Uniform formulation of constitutive laws for clays. In: Desai, C.S., Gallagher, R.H. (Eds.). Mechanics of Engineering Materials. Wiley: Chichester, UK.

[53] Tatlıoğlu, E., Ülker, M.B.C., Lav, A., 2018. Effect of mean stress dependency of elastic soil moduli on the constitutive behavior of sand through UBC-SAND. In Proceedings of the 26th European Young Geotechnical Engineers Conference, Graz, Austria, 11–14 September; pp. 225–234.

[54] Balasubramaniam, A.S., Chaudhry, A.R., 1978. Deformation and strength characteristics of soft Bangkok clay. Journal of Geotechnical Engineering Division (ASCE). 104(9), 1153–1167. DOI: https://doi.org/10.1061/AJGEB6.0000685

[55] Henkel, D.J., 1956. The effect of overconsolidation on the behavior of clays during shear. Géotechnique. 6(4), 139–150. DOI: https://doi.org/10.1680/geot.1956.6.4.139

[56] Taylor, P.W., Bacchus, D.R., 1960. Dynamic cyclic strain tests on clay. In Proceedings of the 7th International Conference on Soil Mechanics and Foundation Engineering, Mexico City, Mexico. pp. 401–409.

[57] Seed, H.B., Lee, K.L., Idriss, I.M., et al., 1973. Analysis of the slides on the San Fernando Dam during the earthquake of Feb. 1971, EERC Report No. EERC73-2. Earthquake Engineering Research Center: Berkeley, CA, USA.

[58] Kuntsche, K., 1982. Tests on clay. In Proceedings of the International Workshop on Constitutive Behavior of Soils, Grenoble, France, 6–8 September 1982.

[59] Duque, J., Roháč, J., Mašín, D., et al., 2022. Experimental investigation on Malaysian kaolin under monotonic and cyclic loading: Inspection of undrained Miner's rule and drained cyclic preloading. Acta Geotechnica. 17, 4953–4975. DOI: https://doi.org/10.1007/s11440-022-01643-0